






InkVis: A High-Particle-Count Approach for Visualization of Phase-Contrast Magnetic Resonance Imaging Data

N. H. L. .C de Hoon¹  and K. Lawonn²  and A.C. Jalba³  and E. Eisemann¹  and A. Vilanova¹ 

¹Department of Intelligent Systems, Delft University of Technology, Delft, The Netherlands

²Institute for Computational Visualistics, University of Koblenz-Landau, Koblenz, Germany

³Department of Mathematics and Computer Science, Eindhoven University of Technology, Eindhoven, The Netherlands

Abstract

Phase-Contrast Magnetic Resonance Imaging (PC-MRI) measures volumetric and time-varying blood flow data, unsurpassed in quality and completeness. Such blood-flow data have been shown to have the potential to improve both diagnosis and risk assessment of cardiovascular diseases (CVDs) uniquely.

Typically PC-MRI data is visualized using stream- or pathlines. However, time-varying aspects of the data, e.g., vortex shedding, breakdown, and formation, are not sufficiently captured by these visualization techniques. Experimental flow visualization techniques introduce a visible medium, like smoke or dye, to visualize flow aspects including time-varying aspects. We propose a framework that mimics such experimental techniques by using a high number of particles. The framework offers great flexibility which allows for various visualization approaches. These include common traditional flow visualizations, but also streak visualizations to show the temporal aspects, and uncertainty visualizations. Moreover, these patient-specific measurements suffer from noise artifacts and a coarse resolution, causing uncertainty. Traditional flow visualizations neglect uncertainty and, therefore, may give a false sense of certainty, which can mislead the user yielding incorrect decisions. Previously, the domain experts had no means to visualize the effect of the uncertainty in the data. Our framework has been adopted by domain experts to visualize the vortices present in the sinuses of the aorta root showing the potential of the framework. Furthermore, an evaluation among domain experts indicated that having the option to visualize the uncertainty contributed to their confidence on the analysis.

CCS Concepts

• *Human-centered computing* → *Scientific visualization*; • *Computing methodologies* → *Scientific visualization*; • *Applied computing* → *Life and medical sciences*;

1. Introduction

Blood flow plays a decisive role in the occurrence and progression of many cardiovascular diseases (CVD's) [HBB*10, MFK*12]. This group of conditions is responsible for the highest mortality and morbidity rates in the world [MBG*15]. The blood flow can be acquired using phase-contrast enhanced magnetic-resonance imaging (PC-MRI). PC-MRI provides blood-flow information that facilitates the understanding and diagnosis of CVD's. These measurements consist of volumetric vector fields that vary in time, capturing quantitative blood-flow information.

The observed patterns in a patient's blood-flow determine the probability of a disease, and, ultimately, can establish a final diagnosis. For example, for certain CVDs, vortex-flow patterns are considered to be an essential factor in the development of these diseases [CCB*05, HH08, KGP*13, AKT*16]. Therefore, visualization of the flow is important, such that it is possible to locate and qualitatively analyze the flow features of interest [CCB*05, HH08, vdGG16]. For the flow visualization often streamlines or pathlines

are [vPBB*10]. However, these visualizations do not capture any of time-varying aspects of the data, such as, how and when vortices form and breakdown, and how they move through the flow (shedding), i.e., information on the evolution of a vortex over time. Which is, for example, important when analyzing the flow in the heart [AKT*16]. An example of vortex formation and breakdown in the aorta with our framework is shown in Fig 1, notice that animation is essential for this type of visualization and is provided in the supporting material. While vortices can be visualized using pathlines, they cannot be used to visually show how they change over time. The pathlines show a static representation of the temporal behaviour of particles, since they only show a single trajectory for a given seeding position, not how this trajectory can change over time. Streaklines, on the other hand, are more adequate to reveal time-varying flow behaviour [Lan96]. To obtain streaklines in physical flows visible foreign material is continuously added. For example, in the medical setting, an angiographic catheter are used to inject contrast dye into the artery to evaluate the flow inside it [CF76]. By continuously seeding particles from a fixed seeding

position, the temporal relation between the particles is maintained and flow changes over time are visually encapsulated. Hence, using streaklines one can recognize both local and global spatial and temporal changes in the flow, that cannot be directly provided by streamlines nor pathlines.

One of the reasons streak visualization is rarely applied for the computer-based visualization of blood flow is that it typically has a higher computer memory footprint, i.e., more temporal data must be available to the visualization. To the best of our knowledge, no system uses streak visualization for PC-MRI data.

Another aspect of PC-MRI data that is often not considered in visualization is the presence of several sources of uncertainty, e.g., phase-wrap artifacts, motion artifacts, partial volume effects and measurement noise, for example, due to inhomogeneity of the magnetic fields. Using traditional flow visualizations, uncertainty is ignored, which can be misleading and generating a false sense of reliability, or it can even cause distrust and conflict. For example, it is known that the presence of measurement noise has a significant influence on the quantification of the vorticity of the flow [vSCG*15]. The flexibility of our framework allows for an interactive uncertainty visualization based on a per-voxel probability distribution, and therefore, presents the user with a way to assess the uncertainty of the flow visualization. Uncertainty analysis is recognized as an essential stage in any decision making process [Fre03], moreover, the visualization of uncertainty is recognized as one of the key challenges in flow visualization [BHJ*14, BAOL12, PV13].

In conclusion, we present a framework for the visualization of PC-MRI data using a high number of mass-less semi-transparent particles. We apply GPU-based particles that are traced and released in parallel to be used in the context of PC-MRI data. The flexibility of our framework allows for various visualization approaches. These include common traditional flow visualizations and adds the possibility for streak visualizations and uncertainty visualizations. The source code and executable of our framework is open source and publicly available at <https://gitlab.com/NielsDeHoon/QFlowExplorer>.

2. Related work

In this section, we present related work on flow and uncertainty visualization since these are the main fields our contributions extend on.

2.1. Flow visualization

In the last years, a focus has been put on identifying and visualizing blood-flow characteristics [KBvP*16, LGP14, VPvP*12] to aid identification of abnormal blood-flow patterns. Many of such flow visualizations are in essence Lagrangian, i.e., mass-less particles advected through the vector field. Often these particle trajectories are shown in the form of lines [vPBB*10] or surfaces [vPBB*11].

In computer-based flow-visualization approaches, experimental visualizations are often mimicked using particles. A method is using Surface Particles [vW92], i.e., particles with a normal vector based on the surface of the particle defined by the flow. Another method is to use semi-transparent textured billboards, where the

density of the particles is proportional to the opacity [KSW04]. More advanced techniques use smoke surfaces [vFWTS08] reconstructed from a high number of particles advected through the flow. To the best of our knowledge, these methods were not yet applied for blood-flow visualization.

Domain experts often use streamlines and pathlines as these provide a static overview of the flow and are commonly used to communicate findings [MFK*12, HH08, KYM*93, vPBB*10]. However, finding the right moment and location for the seeding of the visualization is crucial and non-trivial and choosing the wrong settings can lead to missing essential flow features. One common approach is to place a fixed number of random seeds over space and time that cover the whole vessel. The disadvantages of this approach are that the clutter becomes high, and interpreting the trajectories started at different points in time becomes unfeasible. To understand the temporal behavior of the flow the user has to have a mental map of the various moments in time that are presented. In general, this method of seeding is considered non-optimal [MLP*10]. Streak visualization requires a continuous seeding over time, giving the user a complete overview of the flow along with its temporal behavior. Therefore, streak visualization can be used minimizing the demands on the adequate seed-point definition and facilitating interpretation given the experimental physical flow counterpart.

2.2. Uncertainty of flow data

Several uncertainty-visualization methods have been proposed in the last decades, also specifically for vector fields [GHP*16, HCLS16, OGT11]. However, few have been applied to PC-MRI data.

A first attempt to include uncertainty information in PC-MRI visualizations was presented by Friman et al. [FHH*10]. They have modeled the noise in measured blood-flow unsteady data as a multivariate Gaussian distribution and have presented the uncertainty information using a flow map. They visualize and quantify the uncertainty using conventional flow visualization techniques, such as streamlines and particle traces which often suffers from occlusion. The extension of their work includes pathlines and particle traces. Given some initial conditions, it shows the probability distribution [FHH*11] of a particle passing through a volumetric area, providing a quantitative measure for uncertainty.

Both works by Friman et al. [FHH*10, FHH*11] rely on sequential Monte Carlo sampling of the probability space of the 4D PC-MRI data, which is computationally expensive, hampering interaction. The visualizations proposed by Friman either summarize independent pathlines without indicating the trajectories or only shows pathlines for one seeding position. The work Schwenke et al. [SHFF12] represents the uncertainty by the likeliness of the trajectories using a fast-marching method. However, the technique by Schwenke et al. is non-trivial to extend to unsteady flow, and thus can only capture streamlines. For derived flow features and their uncertainty, the amount of research is still very limited. For the computation of the stroke volume and regurgitation fractions, essential indicators of the effectiveness of the flow, the method by Köhler et al. [KPG*15] takes the uncertainty of the measured data

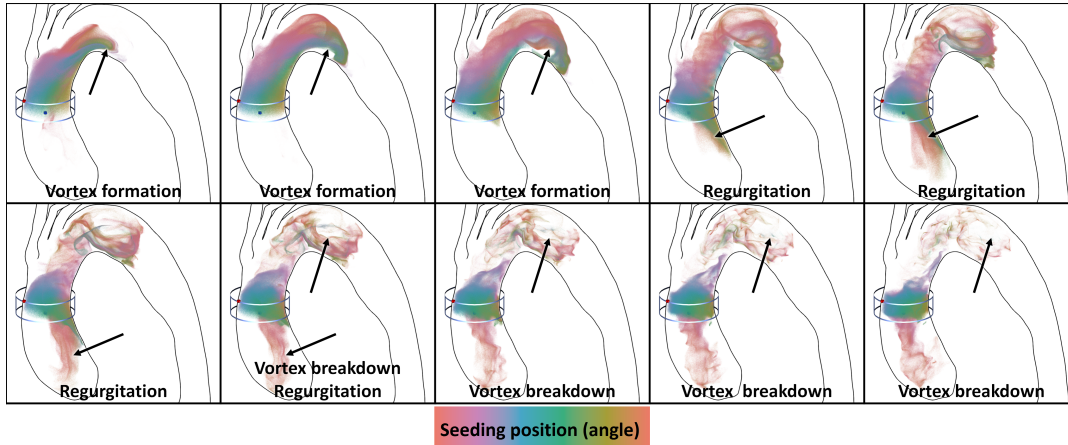


Figure 1: Streak visualization showing the formation, shedding and breakdown of a vortex in a patient with an aortic dissection in the aortic arch and regurgitation is present in the ascending aorta. The corresponding video can be found in the supporting material.

into account to derive robust measures that are insensitive to the correct angulation of the measuring plane. Our method is complementary to the approach by Köhler et al. and could be used as an additional visualization in their context.

Despite the various methods for visualizing the uncertainty of flow that already exist, these methods are not readily suitable for the visualization of the uncertainty of 3D PC-MRI measurements over time at interactive rates. Many of these methods would lead to occlusion and often the relation of the visualization to its seeding position is lost.

In our framework, the measured data is sampled and distorted based on the statistical noise model of Friman et al. [FHH*10, FHH*11]. The modeling itself of the uncertainty is considered out of the scope of this paper, which focuses on the visualization aspects. Our work is based on the assumption that a statistical model of the uncertainty per volumetric position exists. Notice that this excludes the uncertainty in the seeding position, despite its importance [MET*15].

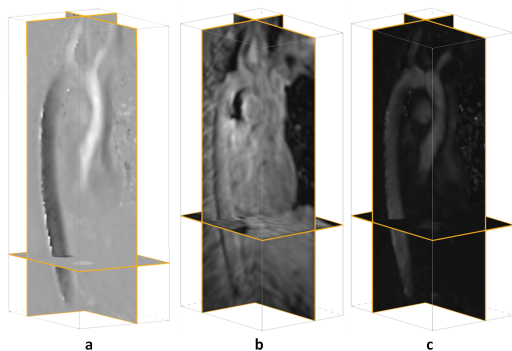


Figure 2: Respectively, one of the three velocity components (inferior to superior) (a), the magnitude (b) and the corresponding signal to noise ratio (c), computed using the method by Friman et al. [FHH*10]. All at peak systole of a healthy volunteer.

3. Data characteristics

For prevention and early diagnosis of symptoms for aortic dissections and other cardiovascular diseases, it is essential to have a good understanding of the flow [HBB*10, MFK*12]. While 4D PC-MRI is not yet used in a clinical setting, research indicates that it provides interesting insights in the blood flow and helps to determine the importance of various flow features [KYM*93, VfDH*18].

For this paper, we use reconstructed PC-MRI data coming directly from the scanner, i.e., without processing it. The vector volumes were cropped around the aorta with a voxel size of $2.0 \times 2.0 \times 2.5$ mm. The acquisitions cover a full heart beat in 20 to 25 phases with a temporal resolution of approximately 40ms. A velocity encoding of a speed of 2m/s was used, with a repetition time (TR) of 4.7ms, echo time (TE) of 2.7ms, and a flip angle of 5° . Fig. 2 shows one of the three velocity components of the phase at peak systole. The vessel segmentation was generated using marching cubes on the temporal maximum intensity projection (TMIP) which is less sensitive to temporally changing noise [KBvP*16]. The resulting mesh was then manually smoothed using mesh-editing software. More details on the acquisition of PC-MRI data are given by Markl et al. [MFK*12] and Gasteiger et al. [Gas14].

4. Mimicking Experimental flow

Our framework is inspired by experimental flow visualization, which often works by injecting a foreign material as a visual medium into the flow, for example, dye or smoke, to create a visual representation of the transport of the material by the flow. The foreign material typically consists of fluid with properties similar to the fluid that is to be inspected.

In computer visualization, we can use a high number of virtual particles to mimic such experimental flow visualizations. By using the GPU, a high amount of particles can be advected in parallel and shown in real time. An efficient implementation of particle advection helps to achieve interactive frame rates [KKKW05]. While such particle systems already exist, some components have to be

adapted to accommodate for use with PC-MRI data. In this section, more details on the particle system are given.

4.1. Integration

In our system, the particles are advected in parallel through the velocity field using a fourth-order Runge-Kutta ODE solver on the GPU. By using the GPU, every particle can be advected in parallel, resulting in interactive frame rates, even for a high number of particles [KKKW05, ELPH18]. The time step is bounded by the Courant-Friedrichs-Lewy (CFL) condition that ensures that a particle moves at most one voxel per time step, t , to reduce the numerical error, i.e.,

$$\Delta t = \frac{voxelSize}{v_{enc}}$$

Here Δt is the maximum safe time step in seconds, $voxelSize$ is the smallest dimension of the voxels in meters, 0.002 meters (2mm) in our data sets, and v_{enc} is an acquisition parameter (in m/s), representing the largest speed that can be measured unambiguously.

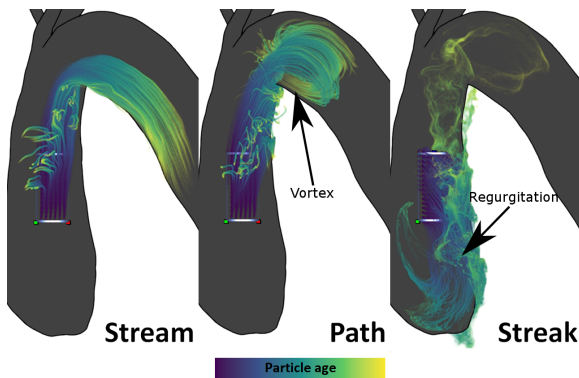


Figure 3: From left to right three line integration options are shown, i.e., stream, path and streak integration. All three methods show different aspects of the flow. The color brightness indicates the age of the particles.

By allowing integration over time and varying the seeding time of the particles, our framework can generate stream- path- and streaklines, as shown in Fig 3, with, from left to right, these three integration options. The stream visualization fails to capture the vortex present in the aortic arch of a patient with an aortic dissection. The path visualization fails to show the regurgitation. However, it clearly indicates the vortex in the arch. The streak visualization does show both the regurgitation in the ascending aorta and the vortex in the aortic arch in a single image.

4.2. Seeding strategies

In both experimental flow visualization and computer-based flow visualization, the seeding positions are a crucial step, which is commonly user-defined. Flow patterns can be missed due to too many seed positions, or insufficiently represented due to too few seed positions or seeding at the wrong position. Notice that in unsteady flow the seeding position includes location and time.

We allow the user to interactively set regions for seeding the

visualization and the number of particles that are seeded per region. The particles are randomly seeded in this area to avoid structured artifacts [vPBB*10]. We also propose to take advantage of the structural artifacts, e.g., by seeding repetitively from a fixed position, it is possible to generate line-like visualizations, thanks to the high number of the particles [KKKW05, ELPH18]. If a single point is used for injecting dye of a given color, the dye will show the flow originating from this point using a line, i.e., a streakline [CF76]. By allowing control on the discontinuity of seeding both on the spatial and temporal seeding location, we can obtain images that are similar to experimental flow visualizations. Some examples of different seeding strategies are shown in Fig 4.

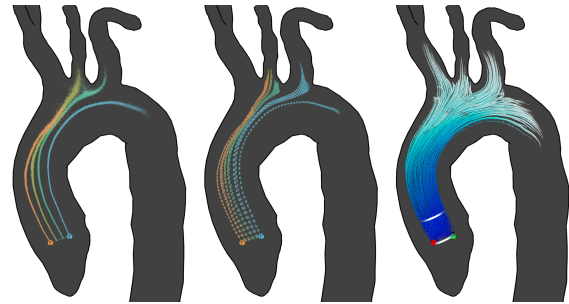


Figure 4: By providing different seeding strategies various flow visualizations can be achieved. In this case a stream visualization. From left to right, an uncertainty visualization with discontinuity on the spatial seeding location, a visualization with discontinuity in both spatial and temporal seeding location, and a volumetric seeding region where particles are seeded from each voxel center.

5. Visual representation

In this section, we describe several visualization strategies that are present in our framework and illustrate the frameworks flexibility. Rendering a large number of particles despite providing flexibility also tends to cause visual clutter. Therefore, we also provide several options to reduce visual clutter.

5.1. Transparency and Depth

Transparency helps to mimic smoke and dye providing some intuitive reference in the analysis. To define the transparency falloff from the particle's center, different kernels could be used. Using a Gaussian kernel yields an ink-like visualization that is applied through this paper. Note that points represent the particles, and, as such, depth sorting can be done for correct transparency by sorting the points based on their distance to the viewer. The sorting and rendering are done on the CPU to enforce a correct rendering order, which would not be guaranteed when the GPU would be used. While the rendering cannot be done in parallel, the system still achieves interactive frame rates.

The transparency can linearly increase depending on the age of the particle: the older the particle, the more transparent it is rendered. Thus, it seems that particles dissolve over time. Having semi-transparent particles is helpful providing a rather global overview of the flow, while an opaque rendering would occlude the structure of the internal flow.

It is essential to be able to correctly identify the shape and spatial position of flow patterns shown by the particle visualization. Therefore, depth encoding is incorporated in our visualizations. Depth darkening by Luft et al. [LCD06] enhances the edges of visualized objects. Based on the relative distance between two points to the viewer, darkening is applied for the farther point. Depth darkening enhances the edges and thus provides a depth cue that has less impact on the underlying color. However, global depth information can be unclear. This method uses the depth buffer, making it non-trivial to apply on transparent renderings, where multiple layers with different depth maps are visible. Therefore, we propose that as we render a particle, we read out the current underlying depth buffer and use the gradient of the depth buffer to decide on the darkness of the particle's halo. This makes it possible to apply depth darkening for transparent particles, which is used for the images in this work. Depth darkening does not interfere with the color of the particles nearest to the viewer and enhances local differences in depth.

5.2. Color traces

Physicians are commonly interested in understanding how the blood flow distributes. Therefore, the user should be able to identify the origin of the particle, to derive the direction and behavior of the flow and patterns in the flow. In physically experimental flow visualization this is done through dye traces. To achieve this effect, we encode the seeding position of each particle using a color, mapped to the seeding positions. All particles emerging from the same location will have the same color and form color traces. We encode the seeding position as a categorical attribute, using color maps with distinctive hues.

We propose to use isoluminant color maps, which makes it possible to use luminance for the visualization of other properties [Bre99]. While the perception of transparency does not rely on the luminance [DCH01], the use of both luminance and transparency are visual channels that interfere with each other. However, for our purpose, the use of transparency is required to regulate the visual clutter and to visualize the complex flow patterns.

For most images in this paper, unless indicated otherwise, an isoluminant color scheme is used. The color schemes were derived from the Hue-Chroma-Lightness (HCL) color space [Iha03], a cylindrical transformation of the CIE $L^*a^*b^*$ color space, such that each equal step through the HCL space results in approximately equal perceptual changes in color.

5.3. Glyph-like visualization

Due to the limited number of available visual channels, it can be helpful to encode certain aspects, for example the speed and direction of the flow, without the use of color. This allows the use of the color channel for encoding different features of the flow. Our framework allows the generation of glyph-like visualizations through applying the shape mapping functions introduced by Evers et al. [EBRI15]. By varying the size of the particle and seeding through time by defining a cyclic pattern we can vary the particle size based on the particle age to obtain a glyph-like representation, as shown in Fig. 5. These glyph-like visualization can be used

to provide additional information regarding, for example, velocity and direction, which does not interfere with both color and opacity encoding [FW89, EBRI15].

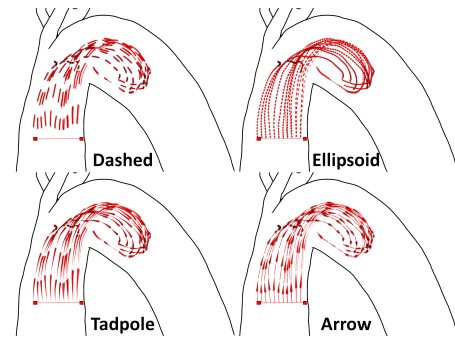


Figure 5: By varying the size of the particles that form a cyclical pattern through time, a glyph-like representation can be achieved, indicating the direction and speed of the flow. The particles are seeded one a line.

6. Uncertainty

The flexibility of our framework allows for the visualization of uncertainty of the flow data. In this paper, uncertainty is seen as the level of robustness of the information provided, such that the user is aware of the randomness present in the data.

This paper does not focus on the derivation of the models that describe these uncertain factors accurately, as this is considered out of scope. Instead, we focus on the visualization of the uncertainty caused by measurement noise, as most previous work. It is important to note that most uncertainty visualizations will not provide extra information to the expert beyond than a level of confidence on the visualization shown. Hence, quantitative assessment is not the goal of such visualization. To convey uncertainty, so-called fuzzy visualization is a common approach [PWL97, KUS*05]. Such fuzzy visualizations make it harder for the user to distinguish for example specific trajectories if the uncertainty is higher, and hence gives an indication of the underlying uncertainty. There is very limited work on showing the effect of the uncertainty in the data. Hence, our goal is to provide this uncertainty information. We focus on measurement noise that is usually modelled through probability distributions. The flow data resulting from PC-MRI measurements is not necessarily divergence-free. As a result, any particle trace in the data is potentially showing non-physical flow. Hence, the idea is that a trace based on the probabilistic distribution of the noise is as valid as a trace based on the acquired PC-MRI data. These probabilistic distributions express the randomness that is present in the scan. It can be seen as that our goal is to visualize the traces that would emerge from multiple scans of the same person and area. Therefore showing the randomness due to acquisition noise.

Despite giving a limited view, measurement noise adds an important source of uncertainty, and the proposed method can be used with other potential models of uncertainty, as long as they are modelled as a distribution that can be sampled. In this section, the derivation and sampling of the distribution of the measurement

noise as will be used in our visualizations is provided. For an estimate of the uncertainty caused by measurement noise, we employ the method presented by Friman et al. [FHH*10], which provides a voxel-wise estimate of the uncertainty.

The Rician noise in PC-MRI data can be approximated by Gaussian noise [GP95] for a high signal-to-noise ratio. This is normally the case for voxels containing blood [FHH*10]. To compute the SNR, we need to estimate the signal strength A and the noise variance σ^2 . For every voxel i , the signal strength is given by

$$A_i = \frac{1}{4} \left(|I_i^O| + |I_i^x| + |I_i^y| + |I_i^z| \right). \quad (1)$$

Here I_i^k , $k \in \{O, x, y, z\}$, is the reconstructed image at voxel i , the superscript O represents Note that the SNR is based on the anatomy and velocity. By doing so low velocity features of the flow within the vessel, such as vortices [BDC14], can From this, we derive a mask Ω that only contains high signal strength voxels, i.e., the non-air voxels. For these voxels, the Rician distribution of the noise in the measurements can be approximated by a Gaussian distribution. The noise variance for all voxels is estimated by

$$\sigma^2 = \frac{1}{|\Omega| - 1} \sum_{i \in \Omega} \left(\frac{1}{3} \sum_{k \in \{0, x, y, z\}} (I_i^k - A_i)^2 \right), \quad (2)$$

where $|\Omega|$ denotes the number of voxels in Ω . Note that we assume that the noise variance is equal for all voxels in the volume, in contrast to the signal strength A , which is derived for each voxel, similar to Friman et al. [FHH*10]. For our data sets, we found an average SNR of approximately 10.

The signal strength is measured by combining the three velocity directions and the magnitude image. From the SNR and the voxel signal strength a covariance matrix is constructed:

$$C_i = \frac{v_{enc}^2}{\pi^2} \cdot \frac{\sigma^2}{A_i^2} \cdot \begin{bmatrix} 2 & 1 & 1 \\ 1 & 2 & 1 \\ 1 & 1 & 2 \end{bmatrix}, \quad (3)$$

where the scalar velocity encoding v_{enc} is an acquisition parameter (in m/s), representing the largest speed that can be measured unambiguously. Then for each measured velocity component in a voxel a Gaussian distribution is defined. We refer to Friman et al. [FHH*10] for more details on the noise model distribution calculation.

6.1. Uncertainty distribution sampling

To visualize uncertainty, we compute random particle trajectories that are defined by sampling the orientation distribution function defined by the uncertainty at each voxel position. These particle trajectories indicate the possible movements that the particles could have taken on a specific scan instance considering the acquisition noise. The noise is assumed to be mutually independent at each voxel. For the computation of the probabilistic particle trajectories, the uncertainty distribution has to be sampled. We apply the same approach as commonly used for stochastic fiber tracking [BWJ*03, SJW*04]. For each integration step, we draw random values from the normal distribution per vector component using the

Box-Muller approach. By randomizing the velocity for every sample based on the signal strength of the voxel and the covariance matrix, the sampling is independent of the time-step size.

From this, we can also compute the difference $diff$ in m/s between the mean velocity vector (\mathbf{vel}_m) and the random velocity vector (\mathbf{vel}_u) obtained by random sampling using the covariance matrix

$$diff = \|\mathbf{vel}_m - \mathbf{vel}_u\|.$$

By accumulating this local difference for each integration step, weighted by the step size in seconds, we obtain a cumulative deviation. This cumulative deviation indicates how much the particle deviates from the measured flow. Hence, if the particle passes through an unreliable voxel the deviation is more likely to be bigger in comparison to when it passes through a more reliable voxel. With an infinite number of particles and a time step that goes to zero we would obtain the true stochastic distribution for a given seeding position. Therefore, we need a high number of particles and a time step that is as small as possible. The user can control both parameters to fine tune the balance between accuracy and performance. Note that, by using the CFL condition for the sample time step size, it is upper bounded and provides results that are comparable to a much smaller time step sizes especially when the certainty is high, as shown in Fig 6 where brighter colors represent a higher cumulative deviation. The user can, however, choose to have higher accuracy of the uncertainty distribution at the cost of performance and thus obtain a better approximation of the stochastic trajectory of a particle when needed, as shown in Fig 6. Note, however, that the visual differences are minimal, suggesting that the CFL condition is a sufficient approximation.

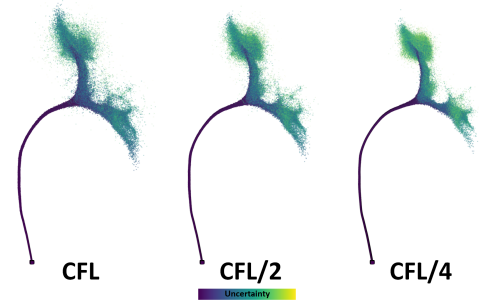


Figure 6: The uncertainty is shown using the Viridis color map. Brighter colors indicate a higher cumulative deviation. Left image: the sample step size is given by the CFL condition; center and right images: the sample step size is set to half and a quarter that by the CFL condition, respectively.

6.2. Uncertainty visual representation

By using isoluminant color schemes, the luminance visual channel can be used to encode the uncertainty. Moreover, the accumulation of luminance indicates a gathering of uncertainty. Note that, if the uncertainty is higher, the visual clutter increases. Additionally, the seeding position becomes difficult to decipher which corresponds unreliability of the information.

For the investigation of the uncertainty it is also possible to map

the transparency of the particle to the accumulated deviation: the more the particle deviates, the more transparent it will be rendered. This allows a reduction of the visibility of the particles that are either older or uncertain.

The cumulative deviation is mapped to the zero-to-one range by dividing it by v_{enc} , i.e., the highest measurable speed. Note that the cumulative deviation is unbounded, so this is a parameter that needs to be tuned. However, this mapping has shown to be robust in our experiments. We use v_{enc} as the upper bound for the cumulative deviation, higher amounts of deviation are shown equal to a deviation of v_{enc} .

Fig 7 shows a streak visualization of systolic flow in a patient with aortic dissection, a vortex can be seen in the aortic arch at phases 10 to 14. The top row shows the measured flow without taking uncertainty into account, while the bottom row shows flow with our uncertainty visualization applied. Here, the cumulative deviation is encoded by an increase of the luminance while the color hue represents the seeding position on the seeding line. The corresponding animation can be found in the supporting information. The animation shows the full heart cycle and shows that the uncertainty is highest during diastole.

7. Flow exploration

The main goal of our framework is to provide tools for gaining insight into the measured PC-MRI flow, for example, its temporal behavior and the influence of uncertainty on the visualization. The massive generation of particles can produce clutter and occlusion especially when uncertainty is considered, and as such interaction is essential.

We provide a filtering mechanism to alleviate the clutter and occlusion generated by the massive amount of particles visualized, which we call particle transfer function. The main idea is to use the concept of transfer functions commonly used in volume rendering. We present a 2D histogram that maps the particle age to the cumulative deviation of the particles. The density in this histogram relates to the number of particles that fall within a range. Using this 2D particle-distribution histogram the distribution of the uncertainty parameters indicates the impact of the uncertainty on the presented visualization of the flow. The uncertainty is increasing monotonically over time, however, the exact form is unknown given that some phases or regions are less reliable than others. The histogram shows the form of this progression and can identify, for example, sudden increases in uncertainty, see Fig 8. The histogram allows, for example, selecting particles that can be considered more reliable due to long age and few deviation, or remove particles that do not contribute to the understanding of the flow.

In Fig 8 and in the supplementary information, an example is shown of the filtering. The particle-distribution histograms depict the amount of the cumulative deviation against the particle age, which can be used to select particles of interest, based on their reliability. Similarly to a transfer function, the user can select particles in the histogram to define its opacity and filter out all other particles, i.e., only the particles that fall into the green box of the graph are shown fully opaque, see Fig 8. In the future, this could be extended with more complex transfer function definitions, i.e., optical

properties such as the color and opacity could be defined based on the selection function. From this, an informed decision on the maximum line length given a seeding area that is reliable can be made, e.g., basing the line length on a maximum cumulative deviation.

The particle-distribution histogram can also be used to filter particles based on their speed, or other properties in relation to the particle age as shown by Fig 9. Some flow properties might work better than others depending on the goal, for example, a general assumption that is often used is that a low-velocity signal means that the data is less reliable. However, some regions, such as the branches of the aorta, have a relatively low-velocity signal, while the magnitude data has a relatively high signal yielding a relatively high SNR. Therefore, in this scenario, filtering based on the cumulative deviation instead of the velocity is most likely to provide a better option as shown by Fig 8 and Fig 9.

Having knowledge of the uncertainty also allows for selectively visualizing only the most certain lines. This is done by ranking each seeding position based on the average deviation of the particles that are emerging from each seeding position. When a high number of random seeding positions is used this filtering can be used to show only the most reliable flow lines, see Figure 10. Moreover, by removing uncertain seeding positions, the amount of clutter caused by the uncertainty visualization can be reduced. The user can interactively change the percentage of lines shown, and thus, they can select a suiting percentage based on their interactive visual analysis.

8. Computational costs

Our method provides an interactive exploration of PC-MRI data. Our GPU implementation allows for advecting more than 2 million particles and rendering them at interactive rates on a system with an Intel Core i7-4770 3.4GHz CPU with 16 gigabytes of memory and an NVidia 760GTX GPU, independent of the size of measurement data and use of uncertainty information. The advection of 2 million particles for a relatively-big time step of one phase (40ms) takes less than two seconds. However, fewer particles are required for an ink-like visualization: typically less than 500.000 particles suffice, for which the system runs at a high frame rate. The rendering performance is linear with the number of particles, e.g., rendering 400.000 or 1 million particles takes respectively 20 and 12 frames per second. The source code and executable of our framework is made public and open source here: <https://gitlab.com/NielsDeHoon/QFlowExplorer>.

9. Results

Several results obtained with our framework have been presented throughout the paper. In this section, we want to extend this results by introducing a use case for which our framework was adopted and an initial user evaluation to measure the potential of the uncertainty visualization aspects of our framework.

9.1. Analysis of aorta root vortices

After being introduced to the framework, the cardiovascular PC-MRI researchers we were collaborating with adopted the framework for the visualization of vortices in the sinuses in the aorta

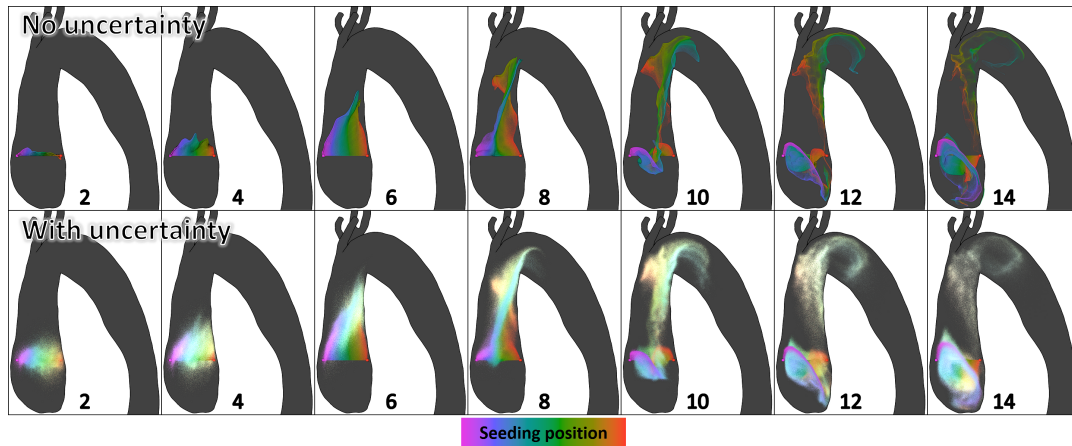


Figure 7: Streak visualization of systolic flow in a patient with an aortic dissection. The bottom row uses our uncertainty visualization. The numbers indicate the current phase of the visualization. Particles leaving the mesh were removed.

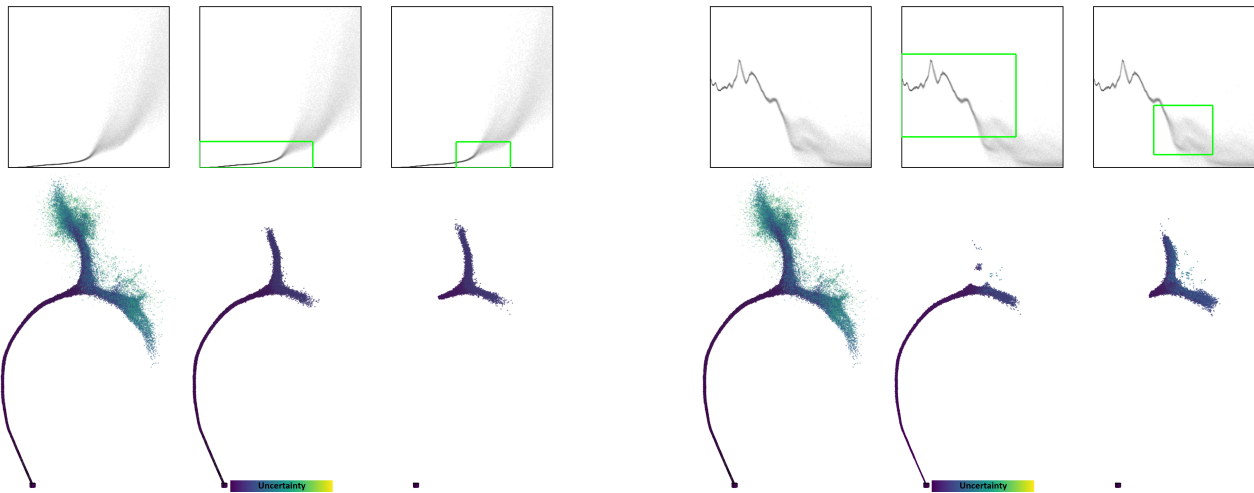


Figure 8: Stream visualization during peak systole. The color shows the cumulative deviation. The cumulative deviation and age of all the particles are shown in the graph on respectively the x and y-axis. Note the sudden increase in deviation in the second half of the histogram. Only the particles that fall in the green box area are rendered.

Figure 9: Stream visualization during peak systole. The color shows the cumulative deviation. The speed and age of all the particles are shown in the graph on respectively the x and y-axis. There is a sudden differences in particle speed that is related to a sudden increase in uncertainty. Only the particles that fall in the green box area are rendered.

root [VFdH*18]. It is thought that these vortices help the leaflets open and close efficiently [BDC14]. Moreover, a correlation between the vortices and calcific aortic valve disease (CAVD) has been found, as is for example demonstrated by Hatoum et al. [HD19] who use two-dimensional in vitro particle image velocimetry (PIV) to generate streak plots. Overall, these vortices play a very important role in the aorta root hemodynamics and the efficiency of the aortic valve.

The cardiovascular PC-MRI researchers are particularly interested in patients that have undergone valve-replacement surgery. They wanted to analyze and compare the flow of 10 healthy volunteers to the flow of 19 patients that had undergone valve-replacement surgery. The goal is to see whether the vortices in the

aorta root are still present after the surgery and whether they differ from healthy volunteers. To do so, the vortices had to be rated based on a semi-quantitative score. Since the vortices form over time they were hard to detect with existing techniques basically due to the difficulty to find the right seeding moment. Streak visualization helps to determine at which phase the vortices are most clearly present, or whether they were present at all.

Using our framework the seeding positions were determined based on the anatomical context and by placing a seeding disk or cylinder through the aorta root while running the streak visualization for the whole heart cycle. An example of such a streak visualization showing the vortices are shown in a video in the supplementary material. Once the phase where the vortices were clearly

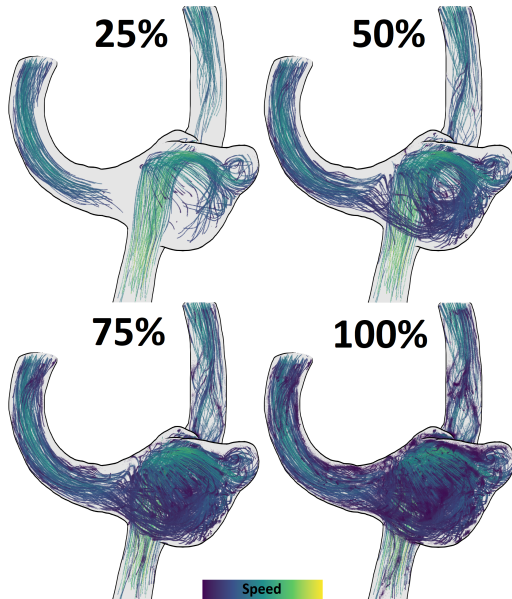


Figure 10: Flow within phantom data of an aneurysm. Each path-line visualization shows a different amount of lines based on the certainty of the lines. The percentage indicates how many seeding positions are used by the visualization after filtering. As such the user can visualize the most reliable flow patterns. Note that the coloring is used to encode the local speed where brighter colors represent higher speeds.

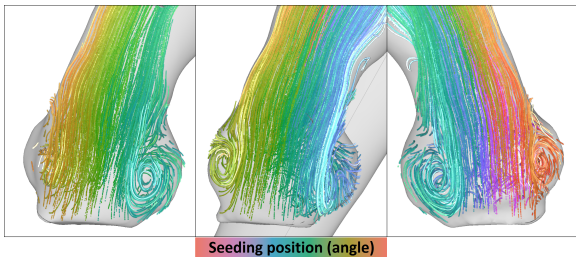


Figure 11: Three vortices in the aorta root were visualized with our framework. These vortices help close the three leaflets of the aortic valve.

visible, if visible at all, is determined, a seeding for streamline visualization is used to produce a still image of each vortex as shown by Fig 11. By filtering based on the viewing direction and the center of the seeding region the amount of clutter could be reduced and the vortex core was seen. For more clarity the vortices were color encoded per sinus based on the seeding position of the particles, while the luminance was mapped to the particle age.

9.2. User evaluation

Full evaluation of the variety of aspects of the presented framework is a complex task that cannot be covered within this paper. Therefore, we have chosen to evaluate the potential of two main aspects of our framework: the importance of using streak visualization to

identify and characterize vortices, and the potential of using the framework for uncertainty visualization.

To evaluate whether streak visualization indeed provided better inside on time-varying aspects of flow we conducted a user study. The study was developed among 24 participants, of which two were cardiovascular PC-MRI researchers. The users were asked to count the number of vortices that formed and broke down over time in an analytic vector field based on an animations showing either pathlines or streaklines. This task is commonly used by clinical researchers to characterize the blood flow, e.g., in the heart or close to the valves [BDC14, AKT*16]. By using an analytic vector field the number of vortices is fixed, thus the performance of the users can be determined by the difference between their count and the actual number of vortices. Overall, the users performed better on this time-varying feature analysis task when a streak visualization was shown, and they also felt more certain on their findings. More information regarding this user study can be found in the additional materials.

We also developed a preliminary user study to evaluate the potential of the uncertainty visualization and exploration provided in our framework. We presented our framework to four cardiovascular PC-MRI researchers who work with this and similar PC-MRI data on a daily basis and are very familiar with flow visualizations. We presented the clinical researchers with a questionnaire that can be found in the supplementary material. The questionnaire was preceded by a demonstration of our visualization using synthetic data with various SNR levels. The user study was conducted in two phases. The first two domain experts were involved in determining the initial requirements for the framework. After they completed the questionnaire changes were made to improve the user study by adding additional questions. The remaining two experts were not involved in the project in any way before filling in the updated questionnaire. Both open questions and questions with respect to users' agreement to a given statement were asked. To determine the agreement a Likert scale was used where the user could indicate their agreement within a range of 1 (negative) to 7 (positive). The questions of the user study are below, note that the additional questions from the second round are indicated by a black triangle instead of an open triangle.

- 1 ▷ Do you think visualization, in general, helps the analysis of blood flow?
- 2 ▷ Do you think uncertainty visualization is helpful for the analysis of blood flow?
- 3 ► Do you understand what the uncertainty visualization represents?
- 4 ▷ Given the knowledge of noise in PC-MRI data, does the uncertainty visualization contribute to your confidence in your analysis?
- 5 ► How does the uncertainty visualization influence your confidence?
- 6 ▷ Can you perceive the various amounts of measurement noise present in the data using the shown visualizations?
- 7 ▷ Would you use this uncertainty visualization?
- 8 ▷ For what type of analysis, if any, would you use the uncertainty visualization?

In a follow up questionnaire the use of filtering based on the un-

certainty included. The users were shown examples of selectively visualizing only the most certain flow patterns before the following questionnaire:

- 9 ► Do you think this type of filtering can be helpful?
- 10 ► Would this type of selection influence your trust in the visualization?
- 11 ► Do you believe this type of filtering will improve your overall analyses?
- 12 ► How do you think the filtering could influence your analyses/conclusions?

The answers of the experts' agreement to the statements are shown in Figure 12. Overall, the domain experts gave positive feedback towards the use of uncertainty visualization and saw a benefit in the visualization of uncertainty. Moreover, they were able to perceive the influence of the noise on the visualization and were more confident with regards to their analysis. Despite the limitations of this study, it indicates the usefulness of visualizing the uncertainty in PC-MRI data. Based on the open question one of the users com-

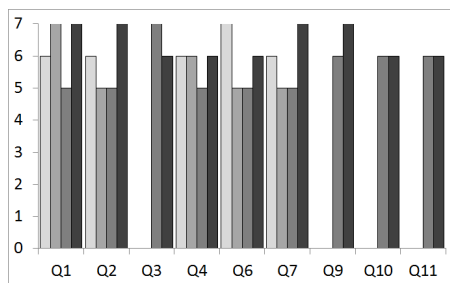


Figure 12: The agreement scores for the user evaluation questions as given by the domain experts using a Likert scale with a range of 1 (negative) to 7 (positive).

mented that the presented visualization would be specifically *interesting for the analysis of flow in an aneurysm or the aorta*. Another participant found that the visualization was useful for the *assessment of vortices (location, type, size and intensity) and wall pressure (location and force)*. Overall all participants were more confident in their analysis and trusted the visualization more. One participant mentioned that it *assists in judging the visualization, in the sense of how much one can "trust" the direction and speed shown*. Experts liked the filtering based on certainty, one mentioned that it helps them *focus on the most essential areas* and noted that *the filtering could be used to explore major flow patterns that can be classified w.r.t. to their influence on disease progression*.

10. Conclusions and Future Work

We have presented a flexible framework inspired by experimental physical flow visualization that allows the visualization of various aspects of blood-flow PC-MRI data. Specifically temporal behaviour and uncertainty are features that can be explored in our proposed framework and that are not commonly available in the currently used methods in PC-MRI visualization.

To mimic experimental flow visualizations, a high number of particles are traced over time through the 3D velocity fields using

existing GPU implementation that has been adapted for PC-MRI data. This allows for traditional stream and path visualizations but also streak visualizations, that can reveal time-varying flow features present in the data. Such features include vortex formation, shedding and breakdown, which are considered important factors in the development of various cardiovascular diseases.

Furthermore, our framework allows for an interactive uncertainty visualization of the flow information and enable the user to explore the uncertainty that is present in the data visually. To mitigate clutter and occlusion, that is often present in 3D flow visualization, we implemented various strategies in our framework, for example, a glyph-like visualization. We also provided interaction techniques such as the particle transfer functions to facilitate filtering and generation of robust visualizations. An initial evaluation among domain experts revealed that our framework is a positive addition to their analysis of the flow. They have also adopted our framework to visualize the vortices that are present in the sinuses of the aorta root.

Although we believe our method improves the understanding of flow patterns and the exploration of blood-flow data, there are several open points which are subject to future work.

To assess the effectiveness of the visualization, a more in-depth user evaluation, including more users would be beneficial. Furthermore, the evaluation of the effectiveness of the glyph-like representation and depth encoding were not considered in our initial evaluation. These techniques were evaluated in a different setting by Evers et al. [EBR15] and Luft et al. [LCD06] respectively. It would be interesting to evaluate their effectiveness within our context. Another valuable addition would be to include feature-based seeding, for example, based on the Lambda2 vortex criterion or the Q-Criterion. We believe this could be especially helpful in combination with filtering the seeding positions such that only the most certain positions are shown to the user.

Since the uncertainty information has not been available to the domain experts before, more evaluation is needed to determine the added value of uncertainty visualization. Furthermore, we focused on the uncertainty due to noise in the measured flow data, while other sources of uncertainty are known to influence the data, such as motion artifacts that occur in the vicinity of the moving cardiac and vessel walls. Another source of uncertainty that could be of interest is the uncertainty resulting from the numerical integration [LPSW96, FBW16, HCLS16]. Another application that would benefit from using uncertainty is the clustering of blood flow patterns that currently do not account for the uncertainty [MVPL18, MOB*19]. By including the uncertainty, the clustering could possibly apply probabilistic similarity measures. Furthermore, it would be interesting to study the modeling of the uncertainty after pre-processing of the measured data using divergence-free filters, and how to ensure and preserve the divergence-free property within our uncertainty visualization framework. Complete modeling of sources of uncertainty is still a complex, open problem. However, all experts participating in the user study indicated that they were more confident in their analysis when the uncertainty was shown and would use the uncertainty visualization.

Finally, it would be interesting to apply our method to differ-

ent flow data sets, such as heart data which develops complex flow patterns in the form of vorticity.

Acknowledgments

We would like to thank dr. ir. A.J. Nederveen and dr. ir. P. van Ooij and from the Radiology department of Amsterdam UMC for sharing his knowledge and data sets.

References

- [AKT*16] ARVIDSSON P. M., KOVACS S. J., TÖGER J., BORGQUIST R., HEIBERG E., CARLSSON M., ARHEDEN H.: Vortex ring behavior provides the epigenetic blueprint for the human heart. In *Scientific reports* (2016), vol. 6. doi:<https://doi.org/10.1038/srep22021>. 1, 9
- [BAOL12] BRODLIE K., ALLENDES OSORIO R., LOPES A.: *A Review of Uncertainty in Data Visualization*. Springer London, London, 2012, ch. 6, pp. 81–109. URL: https://doi.org/10.1007/978-1-4471-2804-5_6, doi:10.1007/978-1-4471-2804-5_6. 2
- [BDC14] BISSELL M. M., DALL'ARPELLINA E., CHOUDHURY R. P.: Flow vortices in the aortic root: in vivo 4D-MRI confirms predictions of Leonardo da Vinci. *European Heart Journal* 35, 20 (2014), 1344. URL: <http://dx.doi.org/10.1093/eurheartj/ehu011>, doi:10.1093/eurheartj/ehu011. 6, 8, 9
- [BHJ*14] BONNEAU G., HEGE H., JOHNSON C., OLIVEIRA M., POTTER K., RHEINGANS P., SCHULTZ T.: *Scientific Visualization: Uncertainty, Multifield, Biomedical, and Scalable Visualization*. Springer London, 2014, ch. Overview and State-of-the-Art of Uncertainty Visualization, pp. 3–27. doi:10.1007/978-1-4471-6497-5_1. 2
- [Bre99] BREWER C.: Color use guidelines for data representation. In *Proceedings of the Section on Statistical Graphics* (1999), American Statistical Association, pp. 55–60. 5
- [BWJ*03] BEHRENS T., WOOLRICH M., JENKINSON M., JOHANSENBERG H., NUNES R., CLARE S., MATTHEWS P., BRADY J., SMITH S.: Characterization and propagation of uncertainty in diffusion-weighted MR imaging. *Magnetic Resonance in Medicine* 50, 5 (2003), 1077–1088. doi:10.1002/mrm.10609. 6
- [CCB*05] CEBRAL J., CASTRO M., BURGESS J., PERGOLIZZI R., SHERIDAN M., PUTMAN C.: Characterization of cerebral aneurysms for assessing risk of rupture by using patient-specific computational hemodynamics models. *American Journal of Neuroradiology* 26, 10 (2005), 2550–2559. URL: <http://www.ajnr.org/content/26/10/2550>. 1
- [CF76] CARROLL R., FALSETTI H.: Retrograde coronary artery flow in aortic valve disease. *Circulation* 54, 3 (1976), 494–499. URL: <http://circ.ahajournals.org/content/54/3/494>, doi:10.1161/01.CIR.54.3.494. 1, 4
- [DCH01] D'ZMURA M., COLANTONI P., HAGEDORN J.: Perception of color change. *Color Research and Application* 26, S1 (2001), S186–S191. doi:10.1002/1520-6378(2001)26:1:5
- [EBR115] EVERTS M., BEKKER H., ROERDINK J., ISENBERG T.: Interactive illustrative line styles and line style transfer functions for flow visualization. *CoRR abs/1503.05787* (2015). 5, 10
- [ELPH18] ENGELKE W., LAWONN K., PREIM B., HOTZ I.: Autonomous particles for interactive flow visualization. *Computer Graphics Forum* 38, 1 (2018), 248–259. URL: <https://onlinelibrary.wiley.com/doi/abs/10.1111/cgf.13528>, arXiv:<https://onlinelibrary.wiley.com/doi/pdf/10.1111/cgf.13528>, doi:10.1111/cgf.13528. 4
- [FBW16] FERSTL F., BÄURGER K., WESTERMANN R.: Streamline variability plots for characterizing the uncertainty in vector field ensembles. *IEEE Transactions on Visualization and Computer Graphics* 22, 1 (Jan 2016), 767–776. doi:10.1109/TVCG.2015.2467204. 10
- [FHH*10] FRIMAN O., HENNEMUTH A., HARLOFF A., BOCK J., MARKL M., PEITGEN H.: Probabilistic 4d blood flow mapping. *MIC-CAI* 13, 3 (2010). doi:10.1007/978-3-642-15711-0_52. 2, 3, 6
- [FHH*11] FRIMAN O., HENNEMUTH A., HARLOFF A., BOCK J., MARKL M., PEITGEN H.: Probabilistic 4d blood flow tracking and uncertainty estimation. *Medical Image Analysis* 15, 5 (2011), 720 – 728. Special Issue on the 2010 Conference on Medical Image Computing and Computer-Assisted Intervention. doi:<http://dx.doi.org/10.1016/j.media.2011.06.002>. 2, 3
- [Fre03] FRENCH S.: Modelling, making inferences and making decisions: The roles of sensitivity analysis. *Top* 11, 2 (2003), 229–251. URL: <http://dx.doi.org/10.1007/BF02579043>, doi:10.1007/BF02579043. 2
- [FW89] FOWLER D., WARE C.: Strokes for representing univariate vector field maps. In *Proceedings of Graphics Interface '89* (1989), GI '89, pp. 249–253. URL: <http://graphicsinterface.org/wp-content/uploads/gi1989-33.pdf>. 5
- [Gas14] GASTEIGER R.: *Visual Exploration of Cardiovascular Hemodynamics*. PhD thesis, Otto-von-Guericke University Magdeburg, 2014. URL: <http://diglib.eg.org/handle/10.2312/8325.3>
- [GHP*16] GUO H., HE W., PETERKA T., SHEN H. W., COLLIS S., HELMUS J.: Finite-time Lyapunov exponents and Lagrangian coherent structures in uncertain unsteady flows. *IEEE Transactions on Visualization and Computer Graphics PP*, 99 (2016). doi:10.1109/TVCG.2016.2534560. 2
- [GP95] GUDBJARTSSON H., PATZ S.: The Rician distribution of noisy MRI data. *Magnetic Resonance in Medicine* 34 (1995). 6
- [HBB*10] HIRATZKA L., BAKRIS G., BECKMAN J., BERSIN R., CARR V., CASEY JR D., EAGLE K., HERMANN L., ISSELBACHER E., KAZEROONI E., KOUCHOUKOS N., LYTLE B., MILEWICZ D., REICH D., SEN S., SHINN J., SVENSSON L., WILLIAMS D.: Guidelines for the diagnosis and management of patients with thoracic aortic disease. *Journal of the American College of Cardiology* 55, 14 (Feb 2010), e27–e129. doi:10.1016/j.jacc.2010.02.015. 1, 3
- [HCLS16] HE W., CHEN C. M., LIU X., SHEN H. W.: A bayesian approach for probabilistic streamline computation in uncertain flows. In *2016 IEEE Pacific Visualization Symposium (PacificVis)* (April 2016), pp. 214–218. doi:10.1109/PACIFICVIS.2016.7465273. 2, 10
- [HD19] HATOUM H., DASI L. P.: Spatiotemporal complexity of the aortic sinus vortex as a function of leaflet calcification. *Annals of Biomedical Engineering* 47, 4 (Apr 2019), 1116–1128. URL: <https://doi.org/10.1007/s10439-019-02224-1>, doi:10.1007/s10439-019-02224-1. 8
- [HH08] HOPE T. A., HERFKENS R. J.: Imaging of the thoracic aorta with time-resolved three-dimensional Phase-Contrast MRI: A review. *Seminars in Thoracic and Cardiovascular Surgery* 20, 4 (2008), 358 – 364. doi:<http://dx.doi.org/10.1053/j.semtcvs.2008.11.013>. 1, 2
- [Iha03] IHAKA R.: Colour for presentation graphics. In *DSC 2003: Proceedings of the 3rd International Workshop on Distributed Statistical Computing* (2003). URL: <http://www.ci.tuwien.ac.at/Conferences/DSC-2003/Proceedings>. 5
- [KBvP*16] KÖHLER B., BORN S., VAN PELT R., HENNEMUTH A., PREIM U., PREIM B.: A survey of cardiac 4D PC-MRI data processing. *Computer Graphics Forum* (2016). URL: <http://dx.doi.org/10.1111/cgf.12803>, doi:10.1111/cgf.12803. 2, 3
- [KGP*13] KÖHLER B., GASTEIGER R., PREIM U., THEISEL H., GUTBERLET M., PREIM B.: Semi-automatic vortex extraction in 4D PC-MRI cardiac blood flow data using line predicates. *IEEE Transactions*

- on *Visualization and Computer Graphics* 19, 12 (Dec 2013), 2773–2782. doi:10.1109/TVCG.2013.189. 1
- [KKKW05] KRÜGER J., KIPFER P., KONCLRATIEVA P., WESTERMANN R.: A particle system for interactive visualization of 3d flows. *IEEE Transactions on Visualization and Computer Graphics* 11, 6 (Nov 2005), 744–756. doi:10.1109/TVCG.2005.87. 3, 4
- [KPG*15] KÖHLER B., PREIM U., GROTHOFF M., GUTBERLET M., FISCHBACH K., PREIM B.: Robust cardiac function assessment in 4d pc-mri data of the aorta and pulmonary artery. *Computer Graphics Forum* 35, 1 (2015), 32–43. doi:10.1111/cgf.12669. 2
- [KSW04] KIPFER P., SEGAL M., WESTERMANN R.: Ueberflow: A gpu-based particle engine. In *Proceedings of the ACM SIGGRAPH/EUROGRAPHICS Conference on Graphics Hardware* (New York, NY, USA, 2004), HWWS '04, ACM, pp. 115–122. URL: <http://doi.acm.org/10.1145/1058129.1058146>, doi:10.1145/1058129.1058146. 2
- [KUS*05] KNISS J., UITERT R. V., STEPHENS A., LI G., TASDIZEN T., HANSEN C.: Statistically quantitative volume visualization. *IEEE visualization* (2005), 287–294. 5
- [KYM*93] KILNER P., YANG G., MOHIADDIN R., FIRMIN D., LONGMORE D.: Helical and retrograde secondary flow patterns in the aortic arch studied by three-directional magnetic resonance velocity mapping. *Circulation* 88 (1993), 2235–2247. doi:10.1161/01.CIR.88.5.2235. 2, 3
- [Lan96] LANE D.: *Visualizing time-varying phenomena in numerical simulations of unsteady flows*. National Aeronautics and Space Administration, 1996. 1
- [LCD06] LUFT T., COLDITZ C., DEUSSEN O.: Image enhancement by unsharp masking the depth buffer. *ACM Transactions on Graphics* 25, 3 (July 2006), 1206–1213. 5, 10
- [LGP14] LAWONN K., GASTEIGER R., PREIM B.: Adaptive surface visualization of vessels with animated blood flow. *Computer Graphics Forum* 33, 8 (2014), 16–27. 2
- [LPSW96] LODHA S. K., PANG A., SHEEHAN R. E., WITTENBRINK C. M.: Uflow: visualizing uncertainty in fluid flow. In *Visualization '96. Proceedings.* (October 1996), pp. 249–254. doi:10.1109/VISUAL.1996.568116. 10
- [MBG*15] MOZAFFARIAN D., BENJAMIN E., GO A., ARNETT D., GLAHA M., CUSHMAN M., DE FERRANTI S., DESPRÄL'S J., FULLERTON H., HOWARD V., MUFFMAN M., JUDD S., KISSELA B., LACKLAND D., ET AL.: Heart disease and stroke statistics—2015 update: a report from the American Heart Association. *Circulation* 131, 4 (Jan 2015), e29–e322. 1
- [MET*15] MCLOUGHLIN T., EDMUNDS M., TONG C., LARAMEE R. S., MASTERS I., CHEN G., MAX N., YEH H., ZHANG E.: Visualization of input parameters for stream and pathline seeding. *International Journal of Advanced Computer Science and Applications* 6 (2015). doi:10.14569/IJACSA.2015.060417. 3
- [MFK*12] MARKL M., FRYDRYCHOWICZ A., KOZERKE S., HOPE M., WIEBEN O.: 4D flow MRI. *Journal of Magnetic Resonance Imaging* 36, 5 (2012), 1015–1036. doi:10.1002/jmri.23632. 1, 2, 3
- [MLP*10] MCLOUGHLIN T., LARAMEE R. S., PEIKERT R., POST F. H., CHEN M.: Over two decades of integration-based, geometric flow visualization. *Computer Graphics Forum* 29, 6 (Sept 2010), 1807–1829. URL: <https://onlinelibrary.wiley.com/doi/abs/10.1111/j.1467-8659.2010.01650.x>, doi:10.1111/j.1467-8659.2010.01650.x. 2
- [MOB*19] MEUSCHKE M., OELTZE-JAFRA S., BEUING O., PREIM B., LAWONN K.: Classification of blood flow patterns in cerebral aneurysms. *IEEE Transactions on Visualization and Computer Graphics* 25, 7 (July 2019), 2404–2418. doi:10.1109/TVCG.2018.2834923. 10
- [MVPL18] MEUSCHKE M., VOSS S., PREIM B., LAWONN K.: Exploration of Blood Flow Patterns in Cerebral Aneurysms during the Cardiac Cycle. *Computers & Graphics* 72 (2018), 12–25. 10
- [OGT11] OTTO M., GERMER T., THEISEL H.: Uncertain topology of 3d vector fields. In *2011 IEEE Pacific Visualization Symposium* (March 2011), pp. 67–74. doi:10.1109/PACIFICVIS.2011.5742374. 2
- [PV13] PELT R. V., VILANOVA A.: Understanding blood-flow dynamics: New challenges for visualization. *Computer* 46, 12 (2013), 60–67. <http://dx.doi.org/10.1109/MC.2013.121>. 2
- [PWL97] PANG T., WITTENBRINK M., LODHA K.: Approaches to uncertainty visualization. *The Visual Computer* 13, 8 (1997), 370–390. URL: <http://dx.doi.org/10.1007/s003710050111>, doi:10.1007/s003710050111. 5
- [SHFF12] SCHWENKE M., HENNEMUTH A., FISCHER B., FRIMAN O.: A novel anisotropic fast marching method and its application to blood flow computation in Phase-Contrast MRI. *Methods of information in medicine* 51, 5 (September 2012). doi:10.3414/ME11.02.0032. 2
- [SJW*04] SMITH S. M., JENKINSON M., WOOLRICH M. W., BECKMANN C. F., BEHRENS T. E., JOHANSEN-BERG H., BANNISTER P. R., LUCA M. D., DROBNJAK I., FLITNEY D. E., NIAZY R. K., SAUNDERS J., VICKERS J., ZHANG Y., STEFANO N. D., BRADY J. M., MATTHEWS P. M.: Advances in functional and structural mr image analysis and implementation as FSL. *NeuroImage* 23 (2004), S208–S219. Mathematics in Brain Imaging. doi:https://doi.org/10.1016/j.neuroimage.2004.07.051. 6
- [vdGG16] VAN DER GEEST R., GARG P.: Advanced analysis techniques for intra-cardiac flow evaluation from 4D flow MRI. *Current Radiology Reports* 4, 38 (2016). doi:AID-10.1007/s40134-016-0167-7. 1
- [VFDh*18] VENDRIK J., FARAG E. S., DE HOON N. H. L. C., KLUIN J., BAAN J.: Presence of aortic root vortex formation after tavi with centera confirmed using 4d-flow magnetic resonance imaging. *The International Journal of Cardiovascular Imaging* (Aug 2018). URL: <https://doi.org/10.1007/s10554-018-1413-2>, doi:10.1007/s10554-018-1413-2. 3, 8
- [vFWTS08] VON FUNCK W., WEINKAUF T., THEISEL H., SEIDEL H.-P.: Smoke surfaces: An interactive flow visualization technique inspired by real-world flow experiments. *IEEE Trans. Vis. Comput. Graph.* 14 (2008), 1396–1403. 2
- [vPBB*10] VAN PELT R., BESCOS J. O., BREEUWER M., CLOUGH R. E., GROLLER M. E., TER HAAR ROMENIJ B., VILANOVA A.: Exploration of 4D MRI blood flow using stylistic visualization. *IEEE Transactions on Visualization and Computer Graphics* 16, 6 (Nov 2010), 1339–1347. doi:10.1109/TVCG.2010.153. 1, 2, 4
- [vPBB*11] VAN PELT R., BESCOS J. O., BREEUWER M., CLOUGH R. E., GROLLER M. E., TER HAAR ROMENIJ B., VILANOVA A.: Interactive virtual probing of 4D MRI blood-flow. *IEEE Transactions on Visualization and Computer Graphics* 17, 12 (Dec 2011), 2153–2162. doi:10.1109/TVCG.2011.215. 2
- [VPvP*12] VILANOVA A., PREIM B., VAN PELT R., GASTEIGER R., NEUGEBAUER M., WISCHGOLL T.: Visual exploration of simulated and measured blood flow. *CoRR abs/1209.0999* (2012). 2
- [vSCG*15] VON SPICZAK J., CRELIER G., GIESE D., KOZERKE S., MAINTZ D., BUNCK A.: Quantitative analysis of vortical blood flow in the thoracic aorta using 4D Phase Contrast MRI. *PLOS ONE* 10, 9 (09 2015), 1–19. doi:10.1371/journal.pone.0139025. 2
- [vW92] VAN WIJK J.: Rendering surface-particles. In *Visualization, 1992. Visualization '92, Proceedings., IEEE Conference on* (Oct 1992), pp. 54–61. doi:10.1109/VISUAL.1992.235226. 2